American Mineralogist, Volume 85, pages 407–419, 2000

A crystal chemical re-evaluation of amphibole/melt and amphibole/clinopyroxene D_{Ti} values in petrogenetic studies

ROBERTA OBERTI,[1,*] RICCARDO VANNUCCI,[1,2] ALBERTO ZANETTI,[1] MASSIMO TIEPOLO,[2] AND RICHARD C. BRUMM[3]

[1] CNR-Centro di Studio per la Cristallochimica e la Cristallografia (CSCC), via Ferrata 1, I-27100 Pavia, Italy
[2] Dipartimento di Scienze della Terra, Università di Pavia, via Ferrata 1, I-27100 Pavia, Italy
[3] Mineralogisch-Petrologisches Institut, Universität Göttingen, Goldschmidtstrasse 1, D-37077 Göttingen, Germany

ABSTRACT

Constraints on the calculation and use of mineral/melt and two-mineral partition coefficients for Ti (D_{Ti}) have been derived from current knowledge of the distinct crystal-chemical mechanisms for the incorporation of Ti^{4+} in the amphibole structure as follows: (1) mineral/melt partition coefficients for Ti, and other tetravalent high field-strength elements (HFSE), can be compared only when considering the fraction of Ti^{4+} that enters the same structural site; (2) accurate two-mineral partition coefficients can be obtained only when considering the fraction of Ti^{4+} that is involved in the same crystal-chemical mechanism in the two relevant phases (i.e., $^{M2}Ti^{4+}$ and $^{M1}Ti^{4+}$ for amphibole and clinopyroxene, respectively).

The complete crystal-chemical characterization of synthetic titanian pargasite and kaersutite and of synthetic richterite (all crystallized under P, T, X, f_{O_2} conditions of interest for upper-mantle studies) shows that the site preference of Zr and Hf differs between the two amphibole compositions; these elements are essentially ordered at M2 in pargasite and kaersutite, but preferentially enter M1 in richterite. In the latter case, Ti segregates into the split M1' site with distorted coordination and shorter Ti-O3 distances, whereas Zr and Hf most likely prefer the larger and more regular M1 site. The observed site preference is strongly controlled by the relative dimensions of the available sites. The crystal-chemical mechanisms that govern the incorporation of octahedral high-charge cations are the local charge balance of $^{[IV]}Al$ (by $R^{3,4+}$ at M2) and of dehydrogenation (by $R^{3,4+}$ at M1); thus the incorporation of Zr and Hf depends on distinct intensive parameters in the two amphibole compositions.

Calculation of partition coefficients and of elastic-site parameters under the assumption that all Ti and other $HFSE^{4+}$ order at the M2 site in amphibole, as is currently done in geochemical studies, is strongly biased. In the presence of significant dehydrogenation, amphibole/melt D_0 values obtained from modeling based on the elastic-strain theory starting from the more-accurate site populations for Ti may be only 1/4 of those obtained by using the total Ti content, and the derived site parameters E and r_0 are more consistent with octahedral coordination. This result has important consequences for the prediction of D values under P-T conditions different from those of the experimental work.

Applying the above concepts to data from natural assemblages, we obtained a significantly narrower (0.3–2.4 vs. 1.5–8.9) and more reasonable range of variation for amphibole/clinopyroxene D_{Ti}. A relationship between these values for D_{Ti} and pressure is also now apparent.

INTRODUCTION

Mineral/melt partition coefficients (D values) play a crucial role in determining the composition of hydrous and anhydrous mantle- and crust-derived magmas; a knowledge of the correct values of D is thus fundamental for deciphering magma evolution. Similarly, two-mineral partition coefficients measured for major and trace elements in coexisting mineral phases are potentially very powerful for the petrogenetic study of metamorphic and igneous rocks. The partitioning behavior of many elements is thus fundamental for describing petrological processes in general, but is crucial when studying mantle processes. Unfortunately, a detailed knowledge of how D values vary as a function not only of P, T, and f_{O_2}, but also of the chemical composition (X) of the system must be achieved to interpret the available data more accurately.

The number of studies of partitioning behavior of major and trace elements under different P-T-X conditions in both natural and synthetic assemblages has increased rapidly in recent years due to the availability of very sensitive analytical equipment [such

*E-mail: oberti@crystal.unipv.it

as the ion microprobe (SIMS) and the laser-ablation ICP-MS microprobe], which allow in situ quantification of most elements of the periodic table down to the ppb level.

However, the correct use of experimentally determined D values is not trivial, especially when a particular constituent can be accommodated at more than one structural site or when its site preference (which may vary as a function of bulk composition and of intensive parameters that govern crystallization) has not been understood in detail. The distribution of chemical constituents between independent structural sites has been addressed before, for example to improve the interpretation of Onuma diagrams and the calculation of solution energies in clinopyroxene, where Mg may be distributed between the M2 and M1 sites (Purton et al. 1996, 1997). To our knowledge, this concept has never be applied to the calculation and use of partition coefficients for Ti, which are particularly important in the interpretation of upper-mantle processes.

When addressing partitioning behavior, amphibole may be regarded as a crucial phase, as it occurs in terrestrial igneous rocks encompassing a very wide range of silica activities. Moreover, amphibole is capable of incorporating nearly all the geochemically important elements due to the availability of sites with different coordination (from 4-fold to 12-fold) and also of different sites with the same coordination in its structure.

The partitioning behavior of Ti in amphibole-bearing systems is particularly difficult to interpret. The available values of amphibole/clinopyroxene D_{Ti} show a large range of variation that cannot be explained on the basis of variations of intensive parameters of crystallization, and an unacceptably large scattering within rocks equilibrated at similar conditions. Systematic work on spinel-facies mantle assemblages carried out at the CSCC has shown that values of amphibole/clinopyroxene D_{Ti} are invariably greater than 1 (in the range 2.7–8.9), and are significantly higher than those measured for rare-earth elements (REE) and Zr (Vannucci et al. 1995; Zanetti et al. 1995). These results are confirmed by some recent studies of trace-element signatures of volatile-bearing minerals from mantle assemblages (Ionov et al. 1997, and references therein). Moreover, the measured amphibole/melt D_{Ti} values also suggest that Ti can be strongly fractionated relative to REE and Zr, which has important implications for the geochemical modeling of petrogenetic processes.

Crystal-chemical common sense would suggest that two-mineral D values should depend on the different affinity of the phases involved for the element under consideration, i.e., on the number of exchange vectors in which the element is involved and on the number of structural sites per formula unit (pfu) that are available for each exchange. The crystal-chemical behavior of Ti^{4+} in clinopyroxene is simple, as Ti^{4+} occurs solely at the unique octahedral M1 site and is involved solely in the $^{M1}Ti^{4+}\,{}^{[4]}Al^{3+}_{2}\,{}^{M1}(Mg,Fe)^{2+}_{-1}\,{}^{[4]}Si^{4+}_{-2}$ exchange vector. The behavior of Ti^{4+} is far more complex in amphibole, where three independent octahedral sites are present and where Ti also has been reported to occur in tetrahedral coordination (albeit only in richterite formed at high *T* and low-to-medium *P* conditions; Oberti et al. 1992). The intensive parameters of crystallization control the available exchange vectors in different ways (see next section for further details); thus the partitioning behavior of Ti in amphibole is complex. Decoupling of the exchange vectors related to $^{[6]}Ti$ partitioning has been observed in magmatic richterite (Hawthorne et al. 1998) and in magmatic pargasite and kaersutite (Zanetti et al. 1995); conversely, the concomitant variation of Ti exchange vectors has been reported in a series of peridotites from the Zabargad Island (Red Sea), which underwent a complex sub-solidus evolution (Zanetti et al. 1994).

The complex distribution of Ti in amphibole also has major implications for the interpretation, modeling, and prediction of the amphibole/melt D values measured for other tetravalent trace elements (mainly Zr and Hf), whose behavior is commonly modeled based on the elastic-strain theory.

Accurate modeling of Ti distribution in amphiboles as a function of all the parameters governing crystallization is thus crucial for estimating and using partition coefficients for Ti correctly. In this paper, we report and discuss new amphibole/melt D values for Ti and the other tetravalent HFSE that have been obtained by systematic syntheses of pargasitic and richteritic amphiboles in equilibrium with residual melts under controlled conditions of crystallization typical of the upper mantle (Brumm 1998; Tiepolo 1999). We exploit the crystal-chemical knowledge obtained at the CSCC on site preference and site assignment of all the major elements in amphibole to provide sound constraints for geochemical interpretation. In particular, we show that only a correct site assignment for Ti allows reliable site parameters to be calculated for incorporation of $HFSE^{4+}$ cations. Lastly, we provide examples of the influence of Ti site partitioning in amphiboles on the calculation and interpretation of amphibole/clinopyroxene D-values in experimental run products and in naturally occurring assemblages.

CRYSTAL-CHEMICAL SETTING

The distinct crystal-chemical roles played by Ti^{4+} in different amphibole compositions been the subject of systematic work on the amphibole database available at the CSCC, which currently contains the results of single-crystal structure refinements and complete chemical analyses of more than 900 naturally occurring and synthetic samples. Data on synthetic amphiboles have been added to have reference points for simple compositions crystallized under controlled conditions. The results are reported in more detail in a series of papers (Oberti et al. 1992; Hawthorne et al. 1993, 1998; Tiepolo et al. 1999) and are briefly summarized below.

Tetravalent Ti can be incorporated into the amphibole structure according to three distinct crystal-chemical mechanisms, which can be expressed by the following exchange vectors: (1) $^{T2}Ti^{4+}\,{}^{T2}Si^{4+}_{-1}$; (2) $^{M1}Ti^{4+}\,{}^{O3}O^{2-}_{2}\,{}^{M1}(Mg,Fe)^{2+}_{-1}\,{}^{O3}OH^{-}_{-2}$; (3) $^{M2,M3}Ti^{4+}\,{}^{T1,T2}Al^{3+}_{2}\,{}^{M2,M3}(Mg,Fe)^{2+}_{-1}\,{}^{T1,T2}Si^{4+}_{-2}$. Mechanisms 1 and 2 are specific to amphibole, whereas mechanism 3 also is active in clinopyroxene [in which case the exchange vector is $^{M1}Ti^{4+}\,{}^{T}Al^{3+}_{2}\,{}^{M1}(Mg,Fe)^{2+}_{-1}\,{}^{T}Si^{4+}_{-2}$].

Among the different amphibole compositions, mechanism 1 is observed only in richterite. The presence of the large Ti^{4+} ion at the T2 site improves the matching of the tetrahedral double chain with the octahedral strip, which in richterite is made up of small tetrahedra (eight Si atoms) and large octahedra (five Mg atoms), respectively. Some stretching and kink-

ing of the tetrahedral double chain can also relieve dimensional strain, and is found in richterites formed at low-to-intermediate *T*. The dimensional strain is exacerbated at high *T*, as the expansion coefficient of the tetrahedra is far smaller than that of the octahedra; significant $^{T2}Ti^{4+}$ (up to 0.40 apfu) is thus present in oxygenian richterites from lamproites, and the preference of Ti^{4+} for tetrahedral coordination, which strongly increases the molar volume, is an inverse function of the pressure (Oberti et al. 1992). Thus the presence of $^{T2}Ti^{4+}$ increases richterite stability to higher *T* at low-to-medium *P* conditions.

In all other amphibole end-members, Ti^{4+} is confined to octahedral coordination. Mechanism 2 is active in all sodic, sodic-calcic, and calcic amphibole compositions (and is far more common than previously supposed). The $^{[6]}Ti^{4+}$ preference for the M1 site is a function of the amount of dehydrogenation and thus of *T* and f_{O_2} conditions. Mechanism 3 is more difficult to decipher; $^{M2}Ti^{4+}$ is commonly present in amphiboles, whereas $^{M3}Ti^{4+}$ has been found only in a few samples of titanian pargasite and kaersutite high that contain $^{[6]}Al$. In these compositions, the presence of $^{[6]}Al \geq 2.0$ apfu and of $^{[6]}Al \sim 1.0$ apfu causes severe underbonding of the oxygen atoms at the O1 and O2 sites, which is compensated by the entry of trivalent cations at the M3 site (Oberti et al. 1995). Therefore, when high *T* increases the Al preference for tetrahedral coordination in amphibole and/or the Fe^{3+} content of the system is low, Ti^{4+}can enter the M3 site (Tiepolo et al. 1999).

The presence of different crystal-chemical mechanisms for Ti^{4+} incorporation in amphibole explains why the (raw) amphibole/clinopyroxene D values calculated from the total Ti^{4+} contents in the two phases are especially high under high-*T* conditions, where dehydrogenation becomes particularly important. However, the involvement of several mechanisms for Ti^{4+} substitution in amphibole also implies that the calculation of values of two-mineral and amphibole/melt D_{Ti} from chemical analyses should be based solely on the populations of the sites relevant to homologous exchange vectors. In contrast, all the available data on amphibole/clinopyroxene as well as on amphibole/melt D_{Ti} (Brenan et al. 1995; LaTourrette et al. 1995; Fujinawa and Green 1997; Klein et al. 1997, and references therein) have been obtained under the assumption that all Ti^{4+} orders at the M2 site in amphiboles.

Experimental procedures

Starting compositions and synthesis conditions

Three different bulk-rock compositions were selected as starting materials: (1) an alkali-olivine basalt from Hessen, Germany (sample 472213a; Wedepohl 1983); (2) a basanite from the Mount Melbourne Volcanic Field, Victoria Land, Antartica (sample WR13-141; Wörner et al. 1989); and (3) a lamproite from melting experiments on MARID compositions (Foley et al. 1996; van der Laan and Foley 1994). These compositions were reproduced by mixing oxides and carbonates of Si, Mg, Fe, Al, Ti, Ca, Na, and K. All carbonates were reduced to oxides by sintering, and a mixture of Fe and Fe_2O_3 was used to obtain appropriate proportions of Fe^{2+} and Fe^{3+}. To maximize the compositional range, the K/(Na+Ca), Mg/(Mg+Fe), Ti/(Ti+Si), and Mg/(Mg+Ti) ratios were varied in the different runs by adding appropriate proportions of the relevant oxides. The starting materials were doped with a mixture of trace elements at abundances designed to achieve optimal analytical conditions with counting statistics of better than 2% during microprobe analysis of the amphibole and glass. Bulk-rock compositions 1 and 2 were also reproduced in an Fe-free system to provide reference samples of simpler composition. Amphibole crystallization was promoted by adding 20 wt% water. Further details on the syntheses, chemical characterization, and structure refinements of this latter Fe-free series are given in Tiepolo et al. (1999).

Experiments were performed at the University of Göttingen with a 22 mm piston-cylinder apparatus with a graphite furnace and CaF_2 as pressure medium. The runs were carried out using the hot-piston-out technique at a pressure of 1.4 GPa. Pressure was calibrated by means of the breakdown of albite to jadeite + quartz (Johannes et al. 1971); no correction for friction was applied. The oxygen fugacity was buffered by the inner graphite capsule, which gives f_{O_2} conditions about 2 log units below FMQ. Temperatures were measured with a Pt-$Pt_{90}Rh_{10}$ thermocouple that is accurate to within ±10 °C. The charges were first brought to super-liquidus conditions (T_{sl}) for 1 hour and then cooled slowly (1–0.5 °C/min) to equilibrium annealing temperatures (T_{eq}) slightly lower than those of the liquidus. The charges were kept at T_{eq} for 13 h and then quenched by switching off the power (the estimated cooling rate is around 900 °C/min). A summary of charge compositions and synthesis conditions for the experiments of this work is reported in Table 1; further details may be obtained from Brumm (1998) and Tiepolo (1999), or from the authors upon request.

The run products are glass and amphibole, with subordinate olivine and clinopyroxene (alkali-basalt and basanite), or clinopyroxene (lamproite). The degree of crystallization is around 50%, and no quench crystals were found in the glass. Equilibrium between amphibole (and clinopyroxene, when present) and melt was checked by traverses during the electron-microprobe analyses of the experimental-run products.

X-ray data collection and structure refinement

Amphibole crystals of dimensions suitable for structure refinement (SREF) were obtained in nearly all the experimental runs. Their crystal quality was assessed using the profile and width of Bragg diffraction peaks. Unit-cell dimensions were calculated from least-squares refinement of the *d* values obtained from 50 rows of the reciprocal lattice by measuring the centroid of gravity of each reflection in the range $-30 < \theta < +30°$. Intensity data were collected for the monoclinic equivalent pairs (*hkl* and $h\bar{k}l$) in the range $2 < \theta < 30°$. Intensities were then corrected for absorption, Lorentz, and polarization effects, averaged, and reduced to structure factors. The structure refinements were performed by using the reflections with $I/\sigma_I \geq 3$ or 5, the threshold chosen so as to obtain at least 900 observed reflections; fully ionized scattering factors of appropriate chemical species were used for non-tetrahedral cationic sites, whereas neutral vs. ionized scattering factors were used for tetrahedral sites and oxygen atoms (Oberti et al. 1992). Unit-cell parameters, R_{obs}, and mean bond distances for the cationic sites are given in Table 2. Final atomic coordinates and anisotropic atomic displacement parameters are listed in Table 3[1];

TABLE 1. Experimental charge compositions and synthesis conditions (°C)

No.	SEQ*	Sample	T_{sl}	T_{eq}	No.	SEQ*	Sample	T_{sl}	T_{eq}	No.	SEQ*	Sample	T_{sl}	T_{eq}
1	835	A-N-melt	1245	1015	13	877	B-T-0.97	1245	1015	25	895	C-K-0.5	1230	1020
2	888	A-N-synth.	1245	1015	14	858	B-M-0.30	1245	1030	26	901	C-K-0.5	1230	1020
3	995	A-K-0.71	1245	1015	15	878	B-M-0.45	1245	1045	27	899	C-T*-0.15	1230	850
4	934	A-K-0.81	1245	1015	16	879	B-M-0.75	1245	1050	28	898	C-T*-0.25	1230	850
5	933	A-K-1.00	1245	1015	17	890	B-M-0.90	1245	1050	29	929	C-M-0.8	1230	850
6	837	A-M-0.45	1245	950	18	864	B-M-1.00	1270	1070	30	936	C-M-0.4	1230	850
7	891	A-M-0.75	1245	1050	19	874	B-M-1.00	1270	1070	31	937	C-N-synth	1230	850
8	884	B-T-0.89	1245	975	20	903	B-K-0.50	1245	1030	32	940	C-T*-0.1	1230	850
9	869	B-T-0.89	1245	1055	21	889	B-K-0.81	1245	1030	33	920	C-K-0.143	1230	850
10	892	B-T-0.94	1245	995	22	897	C-M-0.8	1230	850	34	922	C-K-0.167	1230	850
11	894	B-T-0.94	1245	1055	23	900	C-T*-0.3	1230	850					
12	889	B-T-0.97	1245	975	24	872	C-T*-0.2	1230	850					

Note: The code is built up with the composition of the reference rock (A = akali-olivine basalt 472213a, B = basanite WR13-141, C = MARIDs lamproite), the vector that has been varied [N = natural composition, K = Na/(Na+K), M = Mg/(Mg+Fe), T = (Si/(Si+Ti), T* = Mg/(Mg+Ti)], and the value of the A/(A+B) ratio between the two relevant cations. SEQ* = sequence number in the amphibole database. All experiments at 1.4 GPa.

TABLE 2. Unit-cell parameters, R_{obs}, and mean bond-distances for the cationic sites from single-crystal structure refinement

No.	*a*	*b*	*c*	β	*V*	R_{obs}	<T1-O>	<T2-O>	<M1-O>	<M2-O>	<M3-O>	<M4-O>	<A-O>
1	9.846	18.042	5.316	105.10	911.7	1.9	1.669	1.638	2.081	2.048	2.087	2.486	2.931
2	9.858	18.031	5.307	105.13	910.5	1.4	1.671	1.639	2.080	2.053	2.075	2.487	2.941
3	9.850	18.046	5.316	105.10	912.2	1.9	1.672	1.639	2.083	2.050	2.082	2.487	2.935
4	9.838	18.025	5.308	105.01	909.2	1.9	1.671	1.638	2.082	2.052	2.074	2.486	2.922
5	9.806	18.026	5.308	104.91	906.7	2.0	1.671	1.636	2.077	2.053	2.079	2.483	2.916
6	9.880	18.095	5.322	105.13	918.5	1.6	1.674	1.639	2.090	2.050	2.094	2.492	2.949
7	9.862	18.003	5.296	105.19	907.4	1.7	1.667	1.638	2.071	2.059	2.065	2.491	2.923
8	9.853	18.060	5.314	105.07	913.0	1.7	1.671	1.637	2.083	2.051	2.088	2.490	2.937
9	9.873	18.060	5.315	105.17	914.8	1.6	1.671	1.640	2.079	2.056	2.083	2.496	2.938
10	9.865	18.059	5.314	105.08	914.1	1.6	1.671	1.638	2.083	2.054	2.083	2.493	2.936
11	9.856	18.057	5.316	105.07	913.6	1.5	1.672	1.639	2.080	2.054	2.085	2.492	2.937
12	9.862	18.063	5.319	105.06	915.0	1.7	1.673	1.639	2.088	2.046	2.092	2.492	2.937
13	9.857	18.037	5.310	105.09	911.5	2.0	1.670	1.637	2.086	2.047	2.087	2.488	2.936
14	9.898	18.112	5.324	105.18	921.1	1.6	1.671	1.639	2.088	2.063	2.094	2.501	2.948
15	9.862	18.067	5.316	105.11	914.5	1.6	1.670	1.638	2.082	2.056	2.086	2.494	2.941
16	9.871	18.028	5.307	105.24	911.1	2.2	1.671	1.637	2.075	2.055	2.074	2.494	2.930
17	9.888	18.023	5.308	105.31	912.4	1.5	1.671	1.644	2.072	2.056	2.068	2.496	2.931
18	9.903	18.000	5.304	105.44	911.3	1.4	1.670	1.645	2.071	2.055	2.062	2.496	2.929
19	9.906	18.015	5.296	105.35	911.5	1.8	1.667	1.641	2.070	2.065	2.057	2.499	2.929
20	9.919	18.080	5.313	105.26	919.2	1.4	1.669	1.639	2.084	2.069	2.080	2.502	2.944
21	9.869	18.049	5.310	105.16	912.9	1.7	1.670	1.638	2.080	2.059	2.078	2.494	2.933
22	10.032	18.032	5.284	104.85	924.0	2.9	1.622	1.641	2.076	2.091	2.075	2.564	2.955
23	10.029	18.061	5.296	104.78	927.5	1.5	1.626	1.643	2.072	2.094	2.082	2.569	2.957
24	10.022	18.075	5.300	104.77	928.5	1.9	1.625	1.643	2.067	2.097	2.088	2.576	2.959
25	9.987	18.061	5.298	104.81	923.8	1.8	1.625	1.642	2.061	2.095	2.084	2.569	2.955
26	9.987	18.065	5.298	104.82	924.0	1.7	1.627	1.642	2.059	2.095	2.084	2.568	2.955
27	10.041	18.081	5.300	104.79	930.4	1.5	1.626	1.644	2.074	2.098	2.086	2.573	2.961
28	10.046	18.065	5.297	104.82	929.3	1.3	1.626	1.643	2.076	2.096	2.083	2.570	2.958
29	10.039	18.068	5.298	104.81	929.1	1.8	1.626	1.646	2.073	2.095	2.084	2.571	2.960
30	10.031	18.096	5.299	104.72	930.3	2.3	1.626	1.641	2.072	2.098	2.091	2.577	2.959
31	10.011	18.060	5.297	104.77	926.1	2.0	1.623	1.645	2.064	2.093	2.086	2.572	2.958
32	10.051	18.068	5.295	104.79	929.7	1.7	1.626	1.642	2.078	2.097	2.082	2.572	2.958
33	9.922	18.047	5.297	104.37	918.7	1.7	1.627	1.642	2.069	2.090	2.078	2.559	2.924
34	9.908	18.062	5.307	104.36	920.0	2.2	1.628	1.646	2.059	2.089	2.084	2.563	2.933

observed and calculated structure factors can be obtained from the authors upon request.

Electron- and ion-microprobe analysis

The refined crystals were mounted in epoxy resin, polished, and analyzed by electron- and ion-microprobe techniques to determine concentrations of major elements (by EMP), and of trace and volatile (H, F, Cl) elements (by SIMS). Further details on analytical procedures can be found in Oberti et al. (1992), Ottolini et al. (1995) and Bottazzi et al. (1994). Precision and accuracy of the SIMS analyses are within ±10% above the 1 ppm concentration level and are estimated to be better than ±25% at the 0.01 ppm level. Weight percentages of oxides for major elements are reported in the Appendix.

Complete chemical characterization of all the mineral phases and of coexisting glasses in the experimental charges was also made. No zoning or inhomogeneity of major elements was observed in both the crystals and the adjacent residual glasses, indicating that disequilibrium growth during the experiments was minimal. Amphibole/melt D values were obtained for all elements by comparing their abundance (wt% or ppm) measured at the outer zone of the amphibole crystals and in the coexisting glasses; the results pertinent to this work (for Ti, Zr, and Hf) are reported in Table 4. Amphibole/clinopyroxene D

For copies of Table 3, Document AM-00-035, contact the Business Office of the Mineralogical Society of America (see inside cover of a recent issue for price information). Deposit items may also be available on the American Mineralogist web site at http://www.minsocam.org.

values were also calculated wherever clinopyroxene that crystallized under equilibrium conditions was also available, and those results are reported in Table 5.

Calculation of structural formulae and site populations

Because the H_2O contents were measured directly, structural formulae for the amphibole could be calculated by normalization to 24 (O, OH, F, Cl), with the Fe^{3+}/Fe^{2+} ratio and A-site contents in agreement with SREF results. Group-site populations were obtained by distributing the chemical constituents according to current crystal-chemical knowledge of amphiboles under the constraints of the best fit between the group-site scatterings calculated from the chemical analyses and those obtained from the structure refinement (Δss in the Appendix). This procedure has been applied in a number of papers dealing with amphibole crystal-chemistry published in the last ten years by the Pavia-Winnipeg group, and further details can be found in the papers referenced in the previous sections (e.g., Oberti et al. 1995; Hawthorne et al. 1996). The accuracy of the method can be evaluated from the sum of the differences between the two independent estimates; in the present sampling, the uncertainty varies from 0.38 (over 121.99) to 5.86 (over 151.82) electrons pfu, which corresponds to 0.3 to 3.9%, respectively. This discrepancy is partly due to systematic errors and partly to possible chemical zoning, given that SREF results are averaged over the whole crystal and EMP results are averaged over a finite number of analyzed points. The individual octahedral site populations (and thus the partitioning of $^{[6]}Ti^{4+}$, which is the basis of the present work) were derived by distributing the octahedral cations under the constraints of the SREF results (geometrical parameters and site scatterings) and of the active crystal-chemical mechanisms (e.g., the total extra positive charges provided by Fe^{3+} and Ti^{4+} at the M1 site must equal the residual negative charge on O3 due to dehydrogenation). This latter procedure is not trivial, as the presence of dehydrogenation strongly affects all the <cation-O> octahedral distances. For the present work, we exploited a series of relationships between structural and chemical parameters that have been obtained recently from around 200 partially dehydrogenated amphiboles (10–80% oxy-component) analyzed and refined at the CSCC; the resulting Ti^{4+} distributions are reported in Table 4. A complete structure modeling of dehydrogenation in amphiboles, which could provide a more straightforward and user-friendly procedure to distribute octahedral cations (particularly Ti) is under development, and will be reported and discussed in detail in a forthcoming paper.

Predictive models for mineral/melt D and constraints on their application to amphibole

The relationships among partition coefficients, ionic radii, and ionic charges have been established qualitatively since the work of Onuma et al. (1968). More recently, two nearly simultaneous papers (Beattie 1994; Blundy and Wood 1994, hereafter referred as BW) provided a physical basis to explain these

TABLE 4. Ti site-populations and amphibole/melt D values for Ti, Zr, and Hf

Sample	^{T2}Ti	^{M1}Ti	^{M2}Ti	^{M3}Ti	$^{tot}D_{Ti}$	$^{M1}D_{Ti}$	$^{M2}D_{Ti}$	D_{Zr}	D_{Hf}
1	–	0.36	0.08	–	1.96	1.59	0.37	0.25	0.44
2	–	0.43	0.15	–	2.45	1.81	0.64	0.33	0.47
3	–	0.46	0.12	–	3.86	3.05	0.81	0.46	0.75
4	–	0.44	0.17	–	2.87	2.06	0.80	0.47	0.85
5	–	0.47	0.13	–	2.63	2.05	0.58	0.37	0.65
6	–	0.31	0.12	–	4.65	3.39	1.26	0.50	0.75
7	–	0.30	0.10	–	1.22	0.92	0.31	0.41	0.76
8	–	0.48	0.09	–	3.69	3.10	0.59	0.57	1.02
9	–	0.49	0.15	–	1.92	1.46	0.46	0.40	0.74
10	–	0.45	0.09	–	2.51	2.11	0.40	0.56	0.81
11	–	0.53	0.10	–	2.43	2.04	0.39	0.35	0.50
12	–	0.24	0.10	–	7.96	5.66	2.31	0.70	1.29
13	–	0.31	0.13	–	6.19	4.39	1.79	0.55	1.01
14	–	0.52	0.12	–	2.49	2.04	0.45	0.34	0.55
15	–	0.53	0.10	–	2.31	1.94	0.37	0.44	0.70
16	–	0.45	0.15	0.11	1.98	1.27	0.42	0.26	0.43
17	–	0.42	0.11	0.14	2.07	1.30	0.34	0.51	0.95
18	–	0.32	0.25	0.10	1.78	0.84	0.66	0.47	1.11
19	–	0.30	0.17	0.10	1.16	0.62	0.35	0.53	1.17
20	–	0.38	0.09	–	1.19	0.97	0.23	0.18	0.27
21	–	0.41	0.16	–	1.75	1.26	0.49	0.42	0.68
22	0.17	0.05	0.06	–	0.48	0.09	0.10	0.03	0.05
23	0.26	0.20	0.07	–	0.89	0.34	0.11	0.03	0.05
24	0.24	0.40	0.22	–	1.06	0.50	0.27	0.05	0.10
25	0.26	0.50	0.16	–	0.77	0.42	0.14	0.02	0.04
26	0.26	0.50	0.15	–	0.78	0.43	0.13	0.03	0.04
27	0.26	0.27	0.09	–	0.98	0.43	0.15	0.04	0.08
28	0.21	0.13	0.10	–	0.60	0.18	0.14	0.03	0.07
29	0.26	0.28	0.15	–	0.70	0.28	0.16	0.03	0.05
30	0.15	0.40	0.16	–	1.15	0.64	0.26	0.04	0.07
31	0.15	0.37	0.20	–	1.19	0.61	0.33	0.04	0.06
32	0.14	0.09	0.09	–	0.80	0.22	0.22	0.06	0.10
33	0.25	0.23	0.20	–	0.68	0.23	0.20	0.04	0.06
34	0.28	0.55	0.25	–	1.05	0.53	0.24	0.05	0.06

Note: Ti site-populations (in apfu) are based on the SREF results; amphibole/melt D values based on total Ti ($^{tot}D_{Ti}$), and on site populations ($^{M1}D_{Ti}$ and $^{M2}D_{Ti}$).

TABLE 5. Total and site-specific TiO_2 wt% in amphibole clinopyroxene pairs, and two-mineral D_{Ti} values calculated from the total TiO_2 content (Ti_{tot}) and that at M2 (Ti*) in amphibole

		TiO_2 (wt %)				$^{Amph/Cpx}D_{Ti}$	
		Amph			Cpx		
		Tot	M1	M2	Tot	Ti_{Tot}	Ti*
		Run Products, T_{eq}					
A-N-melt*	1015	4.06	3.02	1.04	1.51	2.69	0.69
A-K-1.00	1015	5.33	4.13	1.20	2.04	2.61	0.59
A-K-0.81	1015	5.44	3.92	1.52	2.32	2.34	0.65
A-M-0.45	950	3.66	2.68	0.98	1.76	2.08	0.56
A-N-melt	1015	3.98	3.23	0.75	1.95	2.04	0.38
B-T-0.89	1035	5.71	4.35	1.36	3.40	1.68	0.40
B-T-0.89	1055	5.72	4.35	1.37	3.83	1.49	0.36
B-T-0.89	975	4.94	4.17	0.77	1.88	2.63	0.41
B-T-0.89	995	4.86	3.94	0.92	2.84	1.71	0.32
B-T-0.94	1015	5.03	4.32	0.71	1.67	3.01	0.43
B-T-0.94	1055	5.59	4.72	0.87	1.98	2.82	0.44
B-T-0.94	975	5.02	3.57	1.45	1.88	2.67	0.77
B-T-0.97	995	2.52	2.12	0.40	0.83	3.04	0.48
B-M-1.00	1030	6.04	3.98	2.06	2.69	2.25	0.77
B-K-0.81	1030	4.20	3.39	0.81	2.07	2.03	0.39
B-M-0.45	1045	5.10	4.28	0.82	2.38	2.14	0.35
B-N-synth	1030	5.09	4.16	0.93	1.63	3.12	0.57
		Natural Samples					
BC-03	sp-web/X	2.75	2.37	0.39	0.41	6.55	0.92
BC-05	sp-web/X	1.87	1.61	0.26	0.43	4.16	0.58
ER-R3/3	sp-pl-lh/M	1.70	1.49	0.21	0.63	8.91	1.89
FR 1	sp-hz/M	5.12	4.03	1.09	0.57	5.46	1.93
Ka111	sp-lh/X	2.81	1.82	0.99	0.51	2.70	0.33
LH12	sp-lh/M	3.89	3.14	0.75	0.56	6.95	1.35
Z2008	sp-web/M	2.62	2.06	0.56	0.53	4.94	1.06
Z2067	sp-pl-lh/M	4.65	3.09	1.56	1.18	3.95	1.33
Z2068	sp-pl-lh/M	4.87	3.11	1.76	0.73	6.71	2.43
Z2070	sp-pl-lh/M	2.39	1.27	1.12	0.68	3.53	1.66
Z2073	sp-pl-lh/M	3.02	2.01	1.01	0.82	3.67	1.23
Z2099	sp-lh/M	1.80	1.02	0.78	0.49	3.64	1.58

Note: Wt% oxides per site have been calculated from crystal-chemical formulae. BC-03 and BC-05 from Zanetti et al., (1995), other samples from Vannucci et al. (1995); hz = harzburgite; lh = lherzolite; M = massif; pl = plagioclase; sp = spinel; X = xenolith; web = websterite.

relationships; they both refer to the lattice-site elastic-strain theory to model the energetics of cation-substitution processes. The two models were later shown to give nearly equivalent (within 10%) results for most cations (Purton et al. 1997) and the BW model was preferred by the scientific community due to its simpler formalism:

$$D_i(P,T,X) = D_0(P,T,X)\exp\left\{\frac{-4\pi E N_A\left[\frac{r_0}{2}(r_i-r_0)^2+\frac{1}{3}(r_i-r_0)^3\right]}{RT}\right\}$$

where the numerator is the equation of Brice (1975), which relates the substitution of an *i* cation with radius r_i for a cation with radius r_0 (ideal for the relevant structural site) to the resulting strain energy stored in the crystal lattice, N_A is Avogadro's number, *E* is the Young's modulus of the site, *R* is the gas constant, and *T* is the absolute temperature (K).

The BW equation allows calculation of the partition coefficient (D_i) of any element (either at the major- or the trace-element level) with ionic radius r_i starting from that (D_0) of an element with ionic radius r_0 that is ideal for the structural site of interest. When at least three partition coefficients of homovalent (1+, 2+, … n+) cations entering the same structural site are known, lattice-site parameters (r_0, D_0, and *E*) can be calculated, and D for other homovalent substituents at the same *P*, *T*, *X* conditions can be predicted. Moreover, the equation allows prediction of D_i under different *P*, *T*, *X* conditions for all the possible substituents, which is particularly important when these conditions cannot be attained experimentally.

However, the BW equation strictly holds only if the following assumptions apply: (1) an isotropic lattice, (2) a spherical site, and (3) closed-shell cations; i.e., in the case of prevailing ionic bonds. The BW model was first shown to hold for closed-shell R^{2+}, and then for REE^{3+} partitioning between melts and plagioclase feldspar (Blundy and Wood 1991), and clinopyroxene (Blundy and Wood 1994; Wood and Blundy 1997). The model also has been tested (using simplifying assumptions about site preference and coordination) on partitioning between: (1) pargasite and andesite melts (Brenan et al. 1995); (2) pargasite + phlogopite and basanite melts (LaTourrette et al. 1995); (3) pargasitic hornblende and quartz-dioritic to tonalitic melts (Klein et al. 1997); and (4) garnets within the Py-Gr join and anhydrous silicate melts (van Westrenen et al. 1999). Its validity also has been proposed to extend to any mineral phase and to most chemical substitutions of relevance for petrological studies (Wood and Blundy 1997).

Although this approach is thus becoming increasingly popular in petrogenetic studies, it has only recently been confronted with the results of structure refinements performed on the analyzed crystals and tempered with crystal-chemical insight concerning fine-scale site preferences for major cations in complex mineral phases (Bottazzi et al. 1999). The combined geo- and crystal-chemical approach provides explanations for the anomalies commonly observed in mineral/melt D_{REE} and for the difference between the observed and calculated amphibole/melt D values discussed by Brenan et al. (1995). This approach is likely to provide interpretation of the wide range of variations in amphibole/clinopyroxene D_{Ti} discussed in the introduction. Noticeably, HFSE represent the most critical case among trace elements because they do not fit the ideal requirements of the BW model (at least Ti^{4+} is known to prefer asymmetric coordination). A careful assessment of the crystal-chemical mechanisms for the incorporation of Ti in the amphibole structure is therefore crucial to a reliable application of the BW model to HFSE partitioning in amphibole.

In the absence of split sites and/or inductive effects due to the composition of the adjacent structural site, the ideal ionic radius r_0 (i.e., the radius of the cation for which the site is not subjected to any strain) can be reasonably approximated by the difference between the mean bond-lengths of the site (<cation-O>) and 1.38 Å, the ionic radius of $^{[IV]}O^{2-}$ (Shannon 1976). This value is certainly only approximate, and has been chosen for consistency with the r_i used in the BW equation [an extensive discussion on the validity of the comparison between r_0 and <cation-O> distances is reported in Bottazzi et al. (1999)]. The site parameter r_0 for the relevant sites and homovalent series (i.e., $^{M4}r_0^{3+}$, $^{A}r_0^{1+}$, $^{M2}r_0^{4+}$) was calculated starting from the amphibole/melt D values measured in this work, and compared to the refined mean bond lengths.

Figure 1 shows the r_0 calculated with the simple but com-

monly used site preferences (LILE^{1+} at $^{[12]}$A, all REE at $^{[8]}$M4, all Ti and HFSE^{4+} at $^{[6]}$M2). Even though the agreement with the ideal trend (the line with slope 1.0 and intercept 1.38 Å) is rather good, systematic shifts are evident. The deviation of the $^{[12]}$A site can be explained by considering that A-site cations are known to segregate at very off-centered sites (A*2* and A*m*) with lower coordination numbers (from eight to ten) and shorter <cation-O> distances. Unfortunately, the use of a more appropriate site preference is not possible in this case, as monovalent cations (Na, K, Rb, Cs) order in different ways as a function of both their dimensions and of the bulk composition (Hawthorne et al. 1996). The shorter r_0 calculated for the $^{[8]}$M4 site has been explained by a fine-scale structural control on REE partitioning, with HREE^{3+} substituting for Mg and Fe^{2+} at the off-centered M4' site with lower coordination numbers; in these cases, fitting over two independent sites (M4 and M4') can be obtained, and the resulting r_0 values approach the ideal dependence (Tiepolo et al. 1998; Bottazzi et al. 1999). The reasons for and the implications of the deviations observed for the octahedral sites can be explained by Ti partitioning and are discussed in the following section.

The influence of Ti partitioning on mineral/melt D values and calculated site parameters

Titanian pargasite and kaersutite

As discussed above, Ti^{4+} is always octahedrally coordinated in these amphibole compositions, and is distributed among three available independent sites. We calculated the elastic-site parameters for $^{[6]}$R^{4+} based on the BW equation starting from the measured amphibole/melt D values for Zr and Hf and from different sets of D_{Ti} values calculated according to three different assumptions (in order of increasing crystal-chemical soundness): (a) ^{M1}Ti = Ti_{tot} or ^{M2}Ti = Ti_{tot}; (b) ^{M1}Ti = ½ $^{O3}O^{2-}$, ^{M2}Ti = Ti_{tot} – ^{M1}Ti; and (c) ^{M1}Ti and ^{M2}Ti from the site populations of this work, i.e., after taking into account the presence of ^{M1,M3}Fe^{3+} and of ^{M3}Ti (Table 4). The changes in the shape of the curve on the Onuma diagram and in the calculated site parameters under the different hypotheses can be dramatic. Examples are given in Figure 2 for pargasite no. 17 and richterite no. 28.

To evaluate the reliability of the results, we systematically compared the calculated r_0 with the <cation-O> distances obtained from the structure refinement. The guiding hypothesis is that the development of a reasonable correlation between the two values should indicate the most likely site preference for Zr and Hf. Figure 3 is an expansion of Figure 1 in the region of the octahedral sites; the black triangles refer to calculations performed for the M1 site, the black circles to those performed for the M2 site (thus the abscissas of the two populations coincide in Fig. 3a), and the open circles to three kaersutites in which significant ^{M3}Ti^{4+} contents have been detected (Tiepolo et al. 1999). The values of r_0 calculated for the M2 site strongly increase within the sequence and approach values compatible with the ideal relation with <M2-O>; also their scattering strongly decreases. No relationship or even an

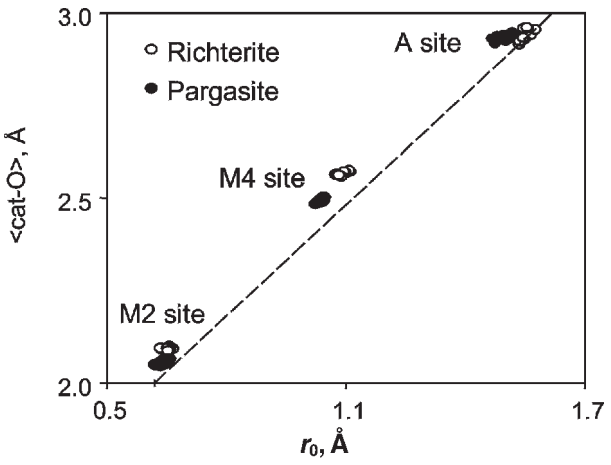

Figure 1. The relationship between r_0 calculated (according to Blundy and Wood 1994) from the measured D values for the relevant substituents at the various group sites with the refined <cation-O> distances. The line is the ideal dependence (slope = 1 and intercept = 1.38 Å).

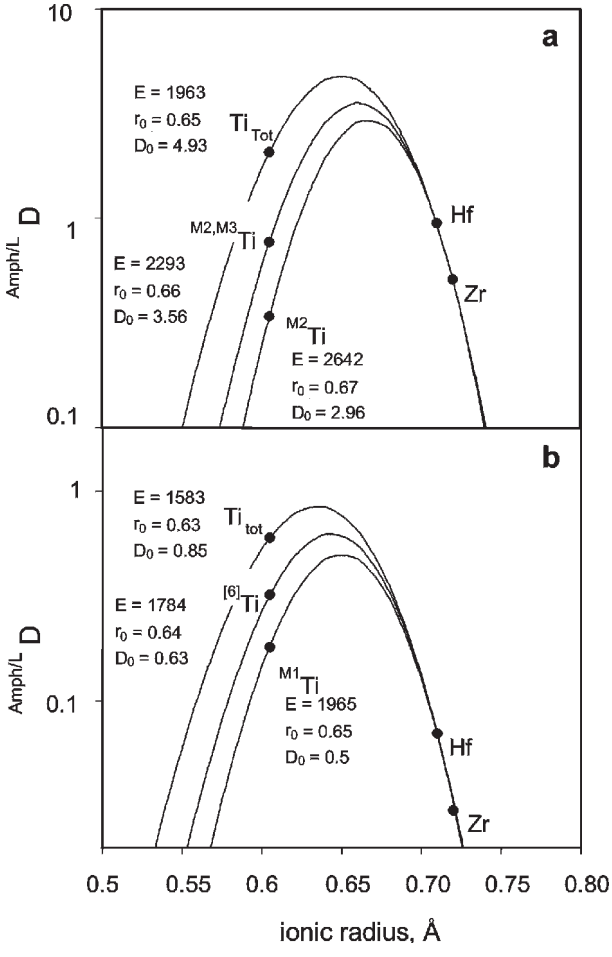

Figure 2. Changes in the Onuma diagram and in the calculated site parameters (Blundy and Wood 1994) obtained by using first the total Ti, Hf, and Zr contents and then increasingly more-refined approximations to the Ti contents at the relevant site (Table 4); (**a**) pargasite no.17; (**b**) richterite no. 28.

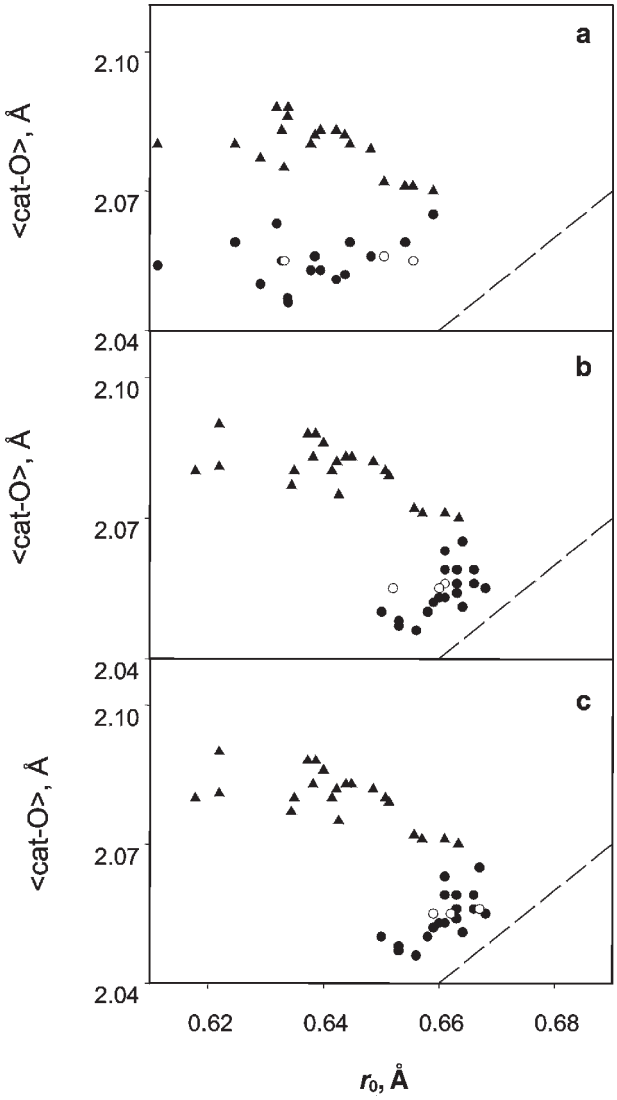

FIGURE 3. Changes in r_0 values calculated from values of D_R^{4+} measured in pargasite and kaersutite according to the different hypotheses of Ti partitioning; (**a**) $^{M1}Ti = Ti_{tot}$ or $^{M2}Ti = Ti_{tot}$; (**b**) $^{M1}Ti = 1/2\ ^{O3}O^{2-}$; $^{M2}Ti = Ti_{tot} - {}^{M1}Ti$; (**c**) ^{M1}Ti and ^{M2}Ti from site populations (Table 4). Symbols: filled triangle = <M1-O>; filled circle = <M2-O>; open circle = Fe-free kaersutite with ^{M3}Ti (Tiepolo et. al. 1999). Line as in Figure 1.

inverse relationship can be observed in the case of the M1 site. Zr and Hf in pargasite and kaersutite thus can be compared with Zr and Hf incorporated into coexisting clinoppyroxene with the aim of providing reliable petrogenetic constraints. This site preference is in accord with the structure refinement of some Zr-rich arfvedsonites from the Motzfeld centre, South Greenland (CSCC, unpublished results). The r_0 values in Figure 3c are still systematically shorter than expected; this is because they are calculated using the ionic radii listed by Shannon (1976), whereas octahedral <cation-O> distances are strongly affected (increased) in dehydrogenated amphiboles, as discussed in a previous section.

Table 6 lists the complete elastic-site parameters calculated under hypotheses (a) and (c) for the pargasites and richterites of the present work. It is also evident that D_0 and E are very sensitive to the assumptions about Ti partitioning. In particular, the D_0 values (i.e., the strain-compensated partition coefficients) obtained with the site-population model are far lower (as little as 1/4) than those calculated with the total Ti content (as is usually done). The E values (which are an inverse measure of the compliance of the site to R^{4+} substitution) increase significantly, and may even double, suggesting that the octahedra are more "rigid" than supposed previously. When calculated with D_{Ti} values from site populations, the E values are in agreement with the few reliable data available for R^{4+} in octahedral coordination, i.e., 2800 and 3400 GPa in two clinopyroxene compositions with high X_{Mg} (Lundstrom et al. 1998). The E values reported by Klein et al. (1997) for synthetic amphiboles crystallized from tonalitic melts (530–850 GPa) are far smaller because the authors assumed that all Ti cations occurred at a unique octahedral site, thus increasing D_0 and decreasing E.

Richterite

Richterite can incorporate Ti^{4+} into sites having tetrahedral and octahedral, and Ti^{4+} may order at the T2 and M1, M2 sites,

TABLE 6. Elastic-site parameters (Blundy and Wood 1994) obtained starting from raw and site-specific values of D_{Ti}

Sample	E, GPa	r_0, Å	D_0	E, GPa	r_0, Å	D_0
			Pargasite			
		Ti tot			Ti at M2	
1	1449	0.64	2.75	2048	0.66	1.50
2	645	0.61	2.45	1119	0.65	1.12
3	1127	0.63	4.45	2041	0.66	2.26
4	1646	0.64	4.92	2113	0.66	3.20
5	1478	0.64	3.86	1661	0.66	2.26
6	726	0.61	4.67	1127	0.65	2.12
7	2060	0.65	3.52	2584	0.67	2.47
8	1535	0.64	5.96	2164	0.66	3.27
9	1879	0.65	4.04	2373	0.66	2.55
10	876	0.63	2.91	1527	0.67	1.58
11	702	0.61	2.44	1350	0.66	1.02
12	1446	0.63	10.43	1992	0.66	5.64
13	1482	0.63	8.09	1917	0.65	4.69
14	1159	0.63	2.98	1816	0.66	1.57
15	1230	0.64	3.10	1912	0.67	1.71
16	1251	0.63	2.44	1812	0.66	1.31
17	1963	0.65	4.93	2642	0.67	2.96
18	2983	0.66	8.84	3386	0.66	6.86
19	2917	0.66	6.96	3372	0.67	5.24
20	899	0.62	1.28	1903	0.66	1.94
21	1371	0.64	2.78	1610	0.66	0.69
			Richterite			
		Ti tot			Ti at M1	
22	1219	0.63	0.55	1772	0.65	0.24
23	520	0.56	1.14	760	0.61	0.35
24	1175	0.62	1.17	1418	0.64	0.74
25	354	0.50	1.78	435	0.54	0.60
26	763	0.59	0.81	891	0.60	0.43
27	1067	0.62	1.02	1331	0.64	0.59
28	1583	0.63	0.85	1965	0.65	0.50
29	1111	0.62	0.73	1410	0.64	0.41
30	1213	0.62	1.21	1396	0.63	0.81
31	671	0.58	1.31	883	0.61	0.62
32	996	0.62	0.85	1401	0.65	0.44
33	451	0.56	0.85	763	0.63	0.25
34	151	0.33	11.49	127	0.36	2.80

respectively. Figure 4 compares the results of the structure refinement with the r_0 calculated starting from the measured values of D_{Zr} and D_{Hf}, and D_{Ti} under the following assumptions: (a) $^{M1}Ti = Ti_{tot}$ or $^{M2}Ti = Ti_{tot}$; (b) $^{M1}Ti = Ti_{tot} - {}^{T2}Ti$; $^{M2}Ti = Ti_{tot} - {}^{T2}Ti$; and (c) the ^{M1}Ti and ^{M2}Ti contents obtained from the structure refinement (Table 4). No relation with the ideal line of slope 1.0 and intercept 1.38 Å is apparent in (a) and (b). In (c) however, where the site populations derived for SREF are taken into account, a trend exists that is consistent with prevalent incorporation at the M1 site. The trend is far less developed than in the case of pargasite and kaersutite, and thus the site preference for Zr and Hf incorporation in richterite is less clear. In particular, the calculated r_0 values are far shorter than the measured ones, especially at high Ti contents, and the slope of the trend is thus different from that of the ideal line. The octahedral relaxation due to dehydrogenation must be invoked as for pargasite. Moreover, the structure refinement of dehydrogenated amphiboles has shown that ^{M1}Ti orders at a split site (M1') at about 0.3–0.4 Å away from the center of the octahedron, which has distorted coordination and shorter distances to the O3 oxygen atoms (Cannillo et al. 1988; Tiepolo et al. 1999). Reasoning based on ionic size suggests that Zr and Hf occur at the center of the M1 octahedron, as the split site occupied by Ti is too small and distorted; thus fitting at M1 on the basis of a single parabola is actually an average over two distinct sites, one of which is smaller than M1. We therefore observe a systematic shift of the calculated r_0 from the reference line (Fig. 4), which becomes increasingly important at high Ti contents, i.e., at higher M1' occupancies. Because the coordination geometry at the M1 site is less suitable for Zr and Hf, these elements are less compatible in richterite than in pargasite and kaersutite, notwithstanding the fact that the ^{M1}Ti contents in the richterite samples of this work are higher than the ^{M2}Ti contents in pargasite and kaersutite (Table 4). It is now clear why unrealistically high D_0 and low E values are obtained for high-Ti samples (Table 6); as in the previous case, the D_0 values calculated under the more-accurate assumptions for Ti partitioning are far lower than those calculated using the total Ti contents.

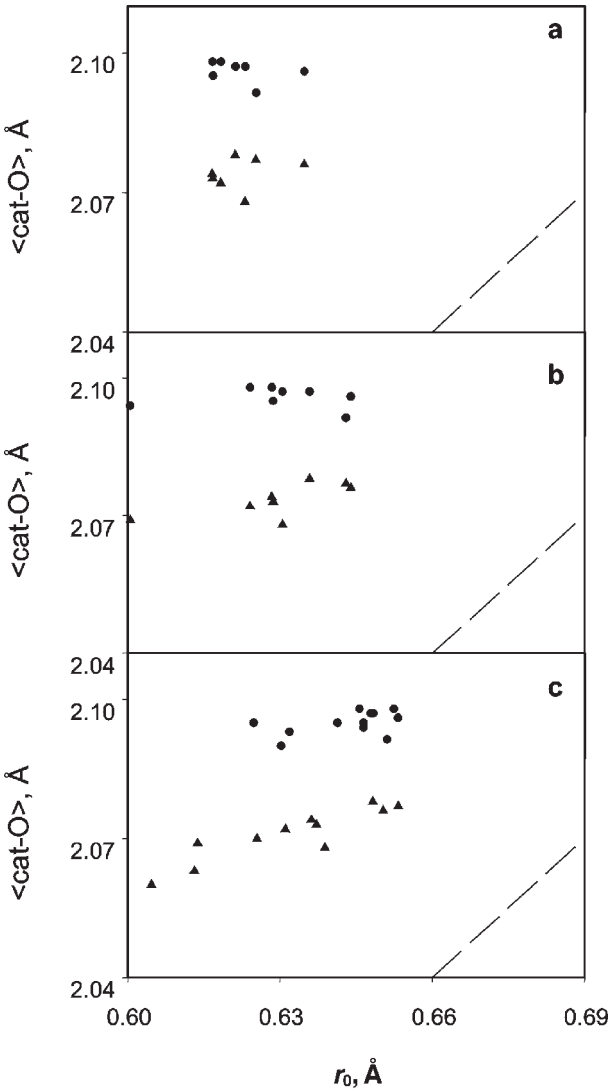

FIGURE 4. Changes in r_0 values calculated from D_R^{4+} measured in richterite according to different hypotheses of Ti partitioning: (**a**) $^{M1}Ti = Ti_{tot}$ or $^{M2}Ti = Ti_{tot}$; (**b**) $^{M1}Ti = Ti_{tot} - {}^{T2}Ti$; $^{M2}Ti = Ti_{tot} - {}^{T2}Ti$; (**c**) ^{M1}Ti and ^{M2}Ti from site populations (Table 4). Symbols and line as in Figure 3. The number of points is higher in (**c**) as the calculation of r_0 under the conditions of (**a**) and (**b**) was impossible or gave unrealistically short values for some samples.

The HFSE preference for the M1 site in richterite is also consistent with the observation that M1 is the smallest octahedral site in richterite, and that the aggregate <M1-O> distances are similar to the <M2-O> distances refined in titanian pargasite and kaersutite. The relationships of Figure 4c do not allow us to exclude the possibility that a smaller fraction of Zr and Hf also enters the M2 site in richterite. In any case, as the entrance of high-charge cations at the M1 site in amphiboles is related to the local balance of dehydrogenation, the D values for Zr and Hf measured in richterite cannot be compared with those measured in clinopyroxene. Concerning D_{Ti}, accurate values can be obtained only after dividing Ti into the fractions occurring at T2, M1, and M2, and only the M2 fraction should be compared to D_{Ti} in coexisting clinopyroxene (D_{Ti}^* in Table 4 and Fig. 5).

Irrespective of the correctness of site assignment, the method proposed in this paper provides reliable site parameters for modeling $HFSE^{4+}$ partitioning in richterite. In the absence of suitable samples from natural rocks, independent information on Zr and Hf site preference in richterite should be obtained from synthesis experiments at proper *P*,*T*,*X* conditions, and these are presently under development in our laboratory.

Implications for models of trace-element behavior in petrogenetic studies

The results reported in this work for $HFSE^{4+}$ and those reported in Tiepolo et al. (1998) and Bottazzi et al. (1999) for REE have shown that the structural peculiarities (i.e., the relative dimensions of the relevant sites) of the individual amphibole compositions under investigation exert stringent controls on both phase partitioning and site preference even at the trace-element level. If we consider that coordination and site preference (degree of order) of some major constituents such as Ti^{4+}

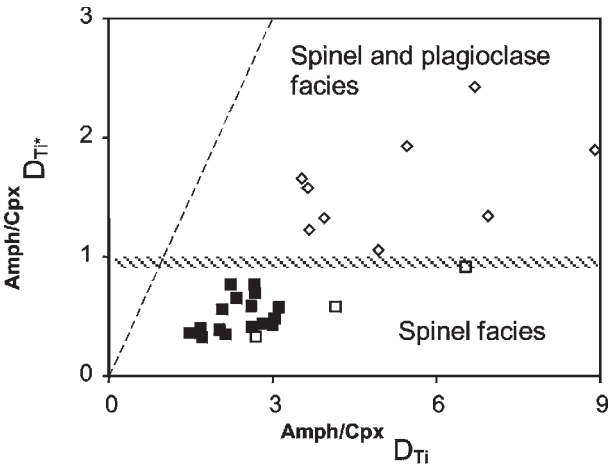

FIGURE 5. Values of $^{Amph/Cpx}D_{Ti}$ for crystals at equilibrium in upper-mantle assemblages (open box = mantle xenoliths, open diamond = peridotite massifs; Vannucci et al. 1995; Zanetti et al. 1995) and in the experimental charges of this work (filled box). D_{Ti} are the raw values, D_{Ti^*} are those calculated from the occupancies of the crystal-chemically analogous sites (M1 in clinopyroxene and M2 in amphibole).

and Al^{3+} (and thus the sizes of the relevant sites at constant overall composition) are a function of the *P-T* (and f_{O_2} for Ti) conditions of equilibration, it is clear that far more compositional parameters must be taken into account and explored in future experimental work to facilitate accurate extrapolation of D values to different *P-T* conditions.

This work shows that the affinity of Zr and Hf for amphibole is definitely lower than expected on the basis of the raw data. The use of mineral/melt D values measured for LILE and HFSE in amphibole (and phlogopite) from basaltic systems has been proposed recently by LaTourrette et al. (1995) to determine the extent to which residual amphibole and phlogopite contribute to the geochemical signature of arc volcanic magmas, and therefore to constrain the origin. The same authors also suggested that D values can be used to test trace-element models of slab melting. In the same way, Klein et al. (1997) suggested that mineral/melt D values measured for amphibole, garnet, and clinopyroxene are relevant to testing models of tonalite genesis. It is now clear that such ambitious goals can be achieved only when the site-specific partitioning behavior of major- and trace-element constituents in any mineral composition are understood as a function of *P*, *T*, *X*, and f_{O_2}.

THE INFLUENCE OF TI PARTITIONING ON AMPHIBOLE/CLINOPYROXENE D_{Ti}

As discussed in the introduction, the few data presently available in the literature on values of amphibole/clinopyroxene D_{Ti} are not easily interpretable. The values obtained by considering the total Ti entering the two phases show a large range of variation (2.7–8.9) and, importantly for petrogenetic studies, these variations cannot be rationalized on the basis of the likely conditions of equilibration (Vannucci et al. 1995; Zanetti et al. 1995; Ionov et al. 1997). The available values from upper-mantle assemblages are reported in Table 5, together with the new ones obtained from some of the experiments described in this work.

Figure 5 compares the "raw" data for amphibole/clinopyroxene D_{Ti} (in the abscissa) with those calculated taking into account only the fractions of Ti that are involved in the same crystal-chemical mechanism, i.e., $^{M2}Ti_{anph}$ and $^{M1}Ti_{cpx}$ (in the ordinate). The latter fall in a more limited range, and allow us to decipher a relationship between the two-mineral D_{Ti} values and petrogenetic conditions. Lower values (0.5–1.0) are recorded in our experiments performed at 1.4 GPa, in spinel-facies lherzolites, and in pyroxenite xenoliths from alkaline lavas. The state of chemical equilibrium between amphibole and clinopyroxene in the synthetic runs in a few cases might be worth more investigation; however, the relatively narrow range of D_{Ti} values observed in samples with large variations in the Ti_{tot} content in both the mineral phases suggests that the site-specific partition coefficients are reliable. A preference for the amphibole phase (D_{Ti} in the range 1–2.5) is observed only in peridotite massifs, either of spinel- or plagioclase-facies. This difference may be related to subsolidus re-equilibration experienced by peridotite massifs during decompression and upwelling. The relationship between amphibole/clinopyroxene D_{Ti} values and *P* is surely worthy of further investigation, but the situation is much clearer when only the fractions of Ti involved in analogous exchange vectors in the two phases are taken into account.

ACKNOWLEDGMENTS

Funding for this work was provided by the Consiglio Nazionale delle Ricerche to the CSCC, by the Ministero della Università e della Ricerca Scientifica e Tecnologica (project "Transformations in subducted materials and mass transfer to the mantle wedge") to Riccardo Vannucci, and by the Deutsche Forschungsgemeinschaft (grant Fo 181/9-1) to Steve Foley. Constructive criticisms from Jon Blundy, Brad Jolliff, and Roger Nielsen helped to improve the manuscript and are gratefully acknowledged.

REFERENCES CITED

Beattie, P. (1994) Systematics and energetics of trace-element partitioning between olivine and silicate melts: implications for the nature of mineral/melt partitioning. Chemical Geology, 117, 57–71.

Blundy, J.D. and Wood, B.J. (1991) Crystal-chemical controls on the partitioning of Sr and Ba between plagioclase feldspar, silicate melts, and hydrothermal solutions. Geochimica et Cosmochimica Acta, 55, 193-209.

———(1994) Prediction of crystal-melt partition coefficients from elastic moduli. Nature, 372, 452-454.

Bottazzi, P., Ottolini, L., Vannucci, R., and Zanetti, A. (1994) An accurate procedure for the quantification of rare earth elements in silicates. In Secondary ion mass spectrometry-SIMS IX, 927-930. Wiley, Chichester.

Bottazzi, P, Tiepolo, M., Vannucci, R., Zanetti, A., Brumm, R.C., Foley, S.F., and Oberti, R. (1999) Distinct site-preference for heavy and light REE in amphibole and the prediction of $^{Amph/L}D_{REE}$. Contributions to Mineralogy and Petrology, 139, 36–65.

Brenan, J.M., Shaw, H.F., Ryerson, F.J., and Phinney, D.L. (1995) Experimental determination of trace-element partitioning between pargasite and a synthetic hydrous andesitic melt. Earth and Planetary Science Letters, 135, 1-11.

Brice, J.C. (1975) Some thermodynamic aspects of the growth of strained cyrstals. Journal of Crystal Growth, 28, 249-253.

Brumm, R. (1998) Die experimentelle Bestimmung von Amphibol/Schmelze-Verteilungskoeffizienten in lamproitischen und lamprophyrischen Systemen. Ph.D. dissertation, 132 p. University of Göttingen.

Cannillo, E., Hawthorne, F.C., Oberti, R., and Ungaretti, L. (1988) Anomalie nella composizione cristallochimica della porzione ottaedrica degli anfiboli. SIMP Annual Meeting, Abstracts, 55 .

Foley, S.F., van der Laan, S.R., and Horn, I. (1996) Major- and trace element compositions of melts from mica-clinopyroxenite in the lower cratonic lithosphereæresults of experiments on mantle vein assemblages. Journal of Conference Abstracts, V.M. Goldschmidt Conference, 1, 172.

Fujinawa, A. and Green, T.H. (1997) Partitioning behaviour of Hf and Zr between

amphibole, clinopyroxene, garnet and silicate melts at high pressure. European Journal of Mineralogy, 9. 379–391.
Hawthorne, F.C., Ungaretti, L., Oberti, R., and Czamanske, G.K. (1993) Li: An important component in igneous alkali amphiboles. American Mineralogist, 78, 733–745.
Hawthorne, F.C., Oberti, R., and Sardone, N. (1996) Sodium at the A site in clinoamphiboles: the effect of composition on patterns of order. Canadian Mineralogist, 34, 577–593.
Hawthorne, F.C., Oberti, R., Zanetti, A., and Czamanske, G.K. (1998) The role of Ti in hydrogen-deficient amphiboles: sodic-calcic and sodic amphiboles from Coyote Peak, California. Canadian Mineralogist, 36, 1253–1265.
Ionov, D.A., Griffin, W.L., and O'Reilly, S.Y. (1997) Volatile-bearing minerals and litophile trace elements in the upper mantle. Chemical Geology, 141, 153–184.
Johannes, W., Bell, P.M., Mao, H.K., Boettcher, A.L., Chipman, D.W., Hays, J.F., Newton, R.C., and Seifert, F. (1971) An interlaboratory comparison of piston-cylinder pressure calibration using the albite breakdown reaction. Contributions to Mineralogy and Petrology, 32, 24–38.
Klein, M., Stosch, H.G., and Seck, H.A. (1997) Partitioning of high-field strength and rare-earth elements between amphibole and quartz-dioritic to tonalitic melts: an experimental study. Chemical Geology, 138, 257–271.
LaTourrette, T., Hervig, R.L., and Holloway, J.R. (1995) Trace element partitioning between amphibole, phlogopite, and basanite melt. Earth and Planetary Science Letters, 135, 13–30.
Lundstrom, C.C., Shaw, H.F., Ryerson, F.J., Williams, Q., and Gill, J. (1998) Crystal chemical control of clinopyroxene-melt partitioning in the Di-Ab-An system: implications for elemental fractionation in the depleted mantle. Geochimica et Cosmochimica Acta, 62, 2849–2862.
Oberti, R., Ungaretti, L., Cannillo, E., and Hawthorne, F.C. (1992) The behaviour of Ti in amphiboles: $^{[IV]}Ti^{4+}$ in richterite. European Journal of Mineralogy, 4, 425–439.
Oberti, R., Hawthorne, F. C., Ungaretti, L., and Cannillo, E.(1995) $^{[6]}Al$ disorder in amphiboles from mantle peridotites. Canadian Mineralogist, 33, 867–878.
Onuma, N., Higuchi, H, Wakita, H., and Nagasawa, H. (1968) Trace element partition between two pyroxenes and the host lava. Earth and Planetary Science Letters, 5, 47–51.
Ottolini, L., Bottazzi, P., Zanetti, A., and Vannucci, R. (1995) Determination of H in silicates by Secondary Ion Mass Spectrometry. Analyst, 120, 1309–1313.
Purton, J.A., Allan, N.L., Blundy, J.D., and Wasserman, E.A. (1996) Isovalent trace element partitioning between minerals and melts: a computer simulation study. Geochimica et Cosmochimica Acta, 60, 4977–4987.
Purton, J.A., Allan, N.L., and Blundy, J.D. (1997) Calculated solution energies of heterovalent cations in forsterite and diopside: implications for trace element partitioning. Geochimica et Cosmochimica Acta, 61, 3927–3936.
Shannon, R.D. (1976) Revised effective ionic radii in oxides and fluorides. Acta Crystallographica, A32, 751–757.
Tiepolo, M. (1999) Determinazione sperimentale dei coefficienti di distribuzione solido/liquido in anfiboli di mantello: ruolo del controllo cristallochimico. Ph.D. dissertation, 314 p. Università di Pavia.
Tiepolo, M., Vannucci, R., Zanetti, A., Brumm, R.C., Foley, S.F., Bottazzi, P., and Oberti, R. (1998) Fine-scale structural control of REE site-preference: the case of amphibole. Mineralogical Magazine, 62A, 1517–1518.
Tiepolo, M., Zanetti, A., and Oberti, R. (1999) Detection, crystal-chemical mechanisms and petrological implications of $^{[6]}Ti^{4+}$ partitioning in pargasite and kaersutite. European Journal of Mineralogy, 11, 345–354.
van der Laan, S.R. and Foley, S.F. (1994) MARIDs and mantle metasomatism. Mineralogical Magazine, 58A, 505–506.
Vannucci, R., Piccardo, G.B., Rivalenti, G., Zanetti, A., Rampone, E., Ottolini, L., Oberti, R., Mazzucchelli, M., and Bottazzi, P. (1995) Origin of LREE-depleted amphiboles in the sub-continental mantle. Geochimica et Cosmochimica Acta, 59, 1763–1771.
van Westrenen, W, Blundy, J., and Wood, B. (1999) Crystal-chemical controls on trace element partitioning between garnet and anhydrous silicate melts. American Mineralogist, 84, 838–847.
Wedepohl, K.H. (1983) Die chemische Zusammensetzung der basaltischen Gesteine der nordlichen Hessichen Senke und ihrer Umgebung. Geologisches Jahrbuch Hessen, 111, 261–302.
Wood, B.J. and Blundy, J.D. (1997) A predictive model for rare earth element partitioning between clinopyroxene and anhydrous silicate melt. Contributions to Mineralogy and Petrology, 129, 166–181.
Wörner, G., Viereck, L., Hertogen, J., Niephaus, H. (1989) The Mt. Melbourne volcanic Field (Victoria Land, Antartica). II. Geochemistry and magma genesis. Geologisches Jahrbuch, 38, 395–433.
Zanetti, A., Sardone, N., Oberti, R., Vannucci, R., Ottolini, L., and Bottazzi, P. (1994) Crystal-chemical changes in amphiboles from Zabargad peridotite: the reconstruction of a complex sub-solidus evolution. 16th IMA General Meeting, Abstracts, 457.
Zanetti, A., Vannucci, R., Oberti, R., and Dobosi, G. (1995) Trace-element compositions and crystal-chemistry of mantle amphiboles from the Carpatho-Pannonian Region. Acta Vulcanologica, 7, 265–276.

MANUSCRIPT RECEIVED JANUARY 20, 1999
MANUSCRIPT ACCEPTED OCTOBER 5, 1999
PAPER HANDLED BY BRAD L. JOLLIFF

Appendix on next page

APPENDIX TABLE 1. Oxide weight percentages from electron- and ion-microprobe analyses, and structural formulae calculated on the basis of 24 (O, OH, F, Cl). A comparison between refined and calculated group-site scatterings (Δss = SREF – EMP) is also given to show the accuracy of the two independent analyses

	1	2	3	4	5	6	7	8	9	10	11	12
SiO_2	40.63	38.06	39.64	39.86	39.36	38.71	40.94	38.73	39.89	40.20	39.24	38.70
TiO_2	3.98	4.98	5.19	5.44	5.33	3.66	3.64	4.94	5.72	4.78	5.59	2.94
Al_2O_3	14.69	15.53	15.44	15.53	14.80	15.40	14.37	14.94	14.53	14.79	15.22	15.16
Cr_2O_3	0.02	0.01	0.01	–	0.01	–	0.02	0.01	–	0.01	0.01	–
FeO(tot)	9.02	15.29	13.80	11.78	12.88	19.72	3.65	16.35	12.94	14.74	13.75	19.06
MnO	0.13	–	0.01	–	0.01	0.01	0.01	0.01	0.01	–	0.01	0.02
MgO	14.11	9.13	10.36	11.18	11.67	6.35	18.20	8.93	11.02	10.50	10.62	8.14
CaO	10.08	9.71	9.91	9.20	8.84	9.95	10.92	9.66	10.28	9.80	9.62	9.58
Na_2O	2.85	2.46	2.80	3.39	3.73	2.55	2.91	2.93	2.75	2.87	2.68	2.96
K_2O	1.14	1.55	1.20	0.75	0.03	1.66	1.23	1.19	1.44	1.12	1.42	1.27
H_2O	1.26	0.95	0.89	1.04	1.01	1.02	1.80	0.99	0.99	1.06	0.90	1.23
F	0.01	0.01	0.03	0.04	0.03	0.21	0.03	0.04	0.04	0.04	0.04	0.06
-O=F	–	–	0.01	0.02	0.01	0.09	0.01	0.02	0.02	0.02	0.01	0.03
Total	97.65	97.80	99.27	98.20	97.69	99.38	97.10	98.74	99.65	99.72	99.11	98.85
Si	6.05	5.88	5.97	6.01	5.96	6.00	5.97	5.93	5.98	6.03	5.92	5.93
Al	1.95	2.12	2.03	1.99	2.04	2.00	2.03	2.07	2.02	1.97	2.08	2.07
Ti	–	–	–	–	–	–	–	–	–	–	–	–
Σ T	8.00	8.00	8.00	8.00	8.00	8.00	8.00	8.00	8.00	8.00	8.00	8.00
Al	0.63	0.70	0.71	0.77	0.60	0.81	0.44	0.62	0.55	0.64	0.63	0.66
Fe^{3+} + Cr	0.20	0.33	0.28	0.05	0.27	0.27	0.07	0.38	0.24	0.21	0.31	0.56
Ti	0.45	0.58	0.59	0.62	0.61	0.43	0.40	0.57	0.65	0.54	0.63	0.34
Mg	2.96	2.02	2.17	2.40	2.47	1.47	3.74	1.95	2.39	2.22	2.27	1.86
Fe^{2+}	0.75	1.37	1.26	1.16	1.05	2.03	0.35	1.48	1.18	1.39	1.16	1.58
Σ M(1,2,3)	5.00	5.00	5.00	5.00	5.00	5.00	5.00	5.00	5.00	5.00	5.00	5.00
Mg	0.17	0.08	0.15	0.11	0.16	0.00	0.21	0.08	0.07	0.13	0.12	0.00
Fe^{2+} + Mn	0.19	0.28	0.20	0.27	0.31	0.26	0.03	0.24	0.21	0.25	0.26	0.30
Ca	1.61	1.61	1.60	1.49	1.43	1.65	1.71	1.58	1.65	1.57	1.56	1.57
Na	0.04	0.04	0.05	0.13	0.10	0.09	0.05	0.10	0.07	0.05	0.06	0.13
Σ M4	2.00	2.00	2.00	2.00	2.00	2.00	2.00	2.00	2.00	2.00	2.00	2.00
Na	0.74	0.70	0.77	0.86	0.99	0.67	0.77	0.77	0.72	0.79	0.73	0.75
K	0.25	0.30	0.23	0.14	0.01	0.33	0.23	0.23	0.28	0.21	0.27	0.25
Σ A	0.99	1.00	1.00	1.00	1.00	1.00	1.00	1.00	1.00	1.00	1.00	1.00
OH	1.25	0.97	0.90	1.04	1.04	1.05	1.75	1.01	0.99	1.06	0.90	1.26
F + Cl	0.01	0.01	0.02	0.03	0.02	0.11	0.02	0.03	0.03	0.03	0.03	0.04
O	0.74	1.02	1.08	0.93	0.94	0.84	0.23	0.96	0.98	0.91	1.07	0.70
Σ X	2.00	2.00	2.00	2.00	2.00	2.00	2.00	2.00	2.00	2.00	2.00	2.00
$\Delta ss_{M(1,2,3)}$	1.69	1.20	2.12	1.25	1.00	4.91	1.00	1.86	0.52	1.61	1.09	1.59
Δss_{M4}	0.85	0.54	0.95	0.59	0.47	0.70	0.54	0.80	0.24	0.73	0.50	0.71
Δss_{A}	0.71	0.29	0.34	–0.09	–0.08	0.25	–0.01	0.49	0.48	0.31	0.28	0.15

	13	14	15	16	17	18	19	20	21	22	23	24
SiO_2	38.61	37.85	37.97	39.75	40.44	40.40	42.39	40.40	39.45	54.10	52.73	51.50
TiO_2	3.84	5.37	5.41	6.35	6.11	6.17	5.22	4.20	5.10	2.66	4.86	7.88
Al_2O_3	15.56	13.85	14.53	14.29	14.36	15.27	13.61	13.41	14.74	0.82	0.93	1.69
Cr_2O_3	0.01	–	–	–	0.02	–	0.02	0.03	0.01	0.03	0.02	0.05
FeO(tot)	16.56	18.33	15.96	7.93	3.77	–	–	12.25	13.70	3.58	5.52	7.82
MnO	0.01	–	–	–	–	–	–	0.01	–	–	–	–
MgO	9.34	6.51	9.14	13.89	16.39	18.39	19.11	12.64	10.91	21.06	18.97	15.84
CaO	9.71	9.98	9.92	10.71	11.01	11.51	11.24	11.19	10.40	7.07	5.88	5.78
Na_2O	2.79	2.59	2.74	2.87	3.16	3.21	3.26	2.36	3.22	3.70	4.14	4.16
K_2O	1.36	1.59	1.53	1.47	1.14	1.16	1.04	1.77	0.94	4.53	4.70	4.70
H_2O	1.25	0.86	0.88	1.08	1.16	1.42	1.45	1.23	1.16	1.99	1.65	1.22
F	0.03	0.06	0.06	0.02	0.02	0.03	0.03	0.02	0.02	0.03	0.03	0.03
-O=F	0.01	0.03	0.03	0.01	0.01	0.01	0.01	0.01	0.01	0.01	0.01	0.01
Total	98.79	98.46	98.13	98.30	97.45	97.56	97.37	99.49	99.48	99.57	99.44	100.65
Si	5.87	6.00	5.84	5.91	5.94	5.86	6.13	6.03	5.90	7.69	7.58	7.47
Al	2.13	2.00	2.16	2.09	2.06	2.14	1.87	1.97	2.10	0.14	0.16	0.29
Ti	–	–	–	–	–	–	–	–	–	0.17	0.26	0.24
Σ T	8.00	8.00	8.00	8.00	8.00	8.00	8.00	8.00	8.00	8.00	8.00	8.00
Al	0.66	0.58	0.47	0.42	0.43	0.47	0.45	0.38	0.50	–	–	–
Fe^{3+} + Cr	0.37	0.31	0.61	0.27	0.25	–	–	0.43	0.40	0.02	0.20	0.01
Ti	0.44	0.64	0.63	0.71	0.67	0.67	0.57	0.47	0.57	0.11	0.27	0.62
Mg	2.12	1.54	2.09	2.98	3.49	3.86	3.98	2.73	2.40	4.46	4.06	3.42
Fe^{2+}	1.41	1.93	1.20	0.62	0.16	–	–	0.99	1.13	0.41	0.47	0.95
Σ M(1,2,3)	5.00	5.00	5.00	5.00	5.00	5.00	5.00	5.00	5.00	5.00	5.00	5.00

(continued on next page)

(continued from preceding page)

Mg	0.00	0.00	0.00	0.10	0.10	0.12	0.14	0.08	0.03	–	–	–
Fe^{2+} + Mn	0.33	0.19	0.25	0.09	0.06	–	–	0.11	0.19	–	–	–
Ca	1.58	1.69	1.63	1.71	1.73	1.79	1.74	1.79	1.67	1.08	0.91	0.90
Na	0.09	0.12	0.12	0.11	0.11	0.09	0.12	0.02	0.11	0.92	1.09	1.10
Σ M4	2.00	2.00	2.00	2.00	2.00	2.00	2.00	2.00	2.00	2.00	2.00	2.00
Na	0.74	0.68	0.70	0.72	0.79	0.81	0.80	0.66	0.82	0.10	0.06	0.07
K	0.26	0.32	0.30	0.28	0.21	0.21	0.19	0.34	0.18	0.82	0.86	0.87
Σ A	1.00	1.00	1.00	1.00	1.00	1.02	0.99	1.00	1.00	0.92	0.92	0.94
OH	1.27	0.91	0.91	1.07	1.14	1.38	1.31	1.22	1.16	1.89	1.58	1.18
F + Cl	0.03	0.04	0.04	0.01	0.01	0.02	0.02	0.01	0.01	0.01	0.01	0.01
O	0.70	1.05	1.05	0.91	0.85	0.61	0.68	0.76	0.83	0.10	0.40	0.80
Σ X	2.00	2.00	2.00	2.00	2.00	2.00	2.00	2.00	2.00	2.00	2.00	2.00
$\Delta ss_{M(1,2,3)}$	1.99	1.40	1.15	–0.80	0.50	0.19	0.20	0.41	–0.04	1.46	2.07	3.42
Δss_{M4}	0.09	0.35	0.21	–0.39	0.26	0.43	0.69	0.19	–0.02	0.01	1.16	0.48
Δss_{A}	1.16	0.07	0.58	0.65	0.67	0.20	0.27	0.12	0.69	0.92	0.93	0.92

	25	26	27	28	29	30	31	32	33	34
SiO_2	51.97	51.86	51.70	52.92	51.96	52.41	52.59	53.05	52.50	52.31
TiO_2	8.41	8.30	5.67	4.00	6.25	6.42	6.52	2.97	6.33	10.06
Al_2O_3	1.25	1.27	1.07	0.88	1.27	0.65	1.18	0.95	1.87	1.65
Cr_2O_3	0.18	0.14	0.01	0.15	0.02	0.01	0.08	0.05	0.08	0.04
FeO(tot)	4.75	4.77	8.18	7.25	4.31	12.50	5.17	8.30	4.30	6.09
MnO	–	–	–	–	–	–	–	–	–	–
MgO	17.34	17.45	16.69	18.01	18.75	13.17	17.56	17.60	19.55	16.02
CaO	5.99	6.07	5.85	6.41	6.37	5.26	5.49	6.03	5.60	4.46
Na_2O	4.02	4.01	4.10	3.93	3.81	4.40	4.27	3.99	6.44	6.57
K_2O	4.75	4.67	4.73	4.61	4.68	4.64	4.74	4.71	1.55	2.36
H_2O	1.00	1.00	1.48	1.79	1.49	1.20	1.27	1.87	1.61	0.92
F	0.09	0.09	0.03	0.03	0.02	0.05	0.08	0.02	0.05	0.07
-O=F	0.04	0.04	0.01	0.01	0.01	0.02	0.03	0.01	0.02	0.03
Total	99.72	99.61	99.51	99.99	98.92	100.70	98.92	99.55	99.86	100.52
Si	7.53	7.52	7.56	7.65	7.53	7.73	7.65	7.70	7.44	7.50
Al	0.21	0.22	0.18	0.15	0.22	0.11	0.20	0.16	0.31	0.28
Ti	0.26	0.26	0.26	0.21	0.25	0.15	0.15	0.14	0.25	0.23
Σ T	8.00	8.00	8.00	8.00	8.00	8.00	8.00	8.00	8.00	8.00
Al	–	–	–	–	–	–	–	–	–	–
Fe^{3+} + Cr	0.02	0.02	0.12	0.02	0.00	0.00	0.01	0.11	0.01	0.01
Ti	0.66	0.64	0.36	0.23	0.43	0.56	0.56	0.18	0.43	0.86
Mg	3.74	3.77	3.63	3.88	4.05	2.89	3.80	3.80	4.05	3.41
Fe^{2+}	0.58	0.57	0.88	0.88	0.52	1.54	0.63	0.90	0.51	0.73
Σ M(1,2,3)	5.00	5.00	5.00	5.00	5.00	5.00	5.00	5.00	5.00	5.00
Mg	–	–	–	–	–	–	–	–	0.07	0.01
Fe^{2+} + Mn	–	0.01	–	–	–	–	0.00	–	–	–
Ca	0.93	0.94	0.92	0.99	0.99	0.83	0.86	0.94	0.85	0.68
Na	1.07	1.04	1.08	1.01	1.01	1.17	1.14	1.06	1.07	1.30
Σ M4	2.00	2.00	2.00	2.00	2.00	2.00	2.00	2.00	2.00	2.00
Na	0.06	0.08	0.08	0.09	0.06	0.09	0.06	0.06	0.70	0.52
K	0.88	0.86	0.88	0.85	0.86	0.87	0.88	0.87	0.28	0.43
Σ A	0.94	0.95	0.96	0.94	0.92	0.96	0.94	0.93	0.98	0.95
OH	0.97	0.97	1.44	1.72	1.44	1.18	1.23	1.81	1.52	0.88
F + Cl	0.04	0.04	0.01	0.01	0.01	0.02	0.04	0.01	0.02	0.03
O	0.99	0.99	0.54	0.26	0.55	0.80	0.73	0.18	0.46	1.09
S X	2.00	2.00	2.00	2.00	2.00	2.00	2.00	2.00	2.00	2.00
$\Delta ss_{M(1,2,3)}$	1.33	1.59	2.12	0.60	2.18	0.21	2.02	2.24	1.97	0.15
Δss_{μ}	0.87	0.37	0.83	0.84	0.33	1.01	0.66	0.99	0.82	–0.05
Δss_{A}	0.71	0.73	0.45	0.80	1.23	0.32	0.78	1.05	0.35	0.28